

Uncertainties in WIMP dark matter scattering revisited

John Ellis^{1,2,3}, Natsumi Nagata⁴, Keith A. Olive^{5,a}

¹ Theoretical Particle Physics and Cosmology Group, Department of Physics, King's College London, London WC2R 2LS, UK

² Theoretical Physics Department, CERN, 1211 Geneva 23, Switzerland

³ National Institute of Chemical Physics and Biophysics, R  vala 10, 10143 Tallinn, Estonia

⁴ Department of Physics, University of Tokyo, Bunkyo-ku, Tokyo 113-0033, Japan

⁵ William I. Fine Theoretical Physics Institute, School of Physics and Astronomy, University of Minnesota, Minneapolis, MN 55455, USA

Received: 1 June 2018 / Accepted: 2 July 2018 / Published online: 11 July 2018
   The Author(s) 2018

Abstract We revisit the uncertainties in the calculation of spin-independent scattering matrix elements for the scattering of WIMP dark matter particles on nuclear matter. In addition to discussing the uncertainties due to limitations in our knowledge of the nucleonic matrix elements of the light quark scalar densities $\langle N | \bar{u}u, \bar{d}d, \bar{s}s | N \rangle$, we also discuss the importances of heavy quark scalar densities $\langle N | \bar{c}c, \bar{b}b, \bar{t}t | N \rangle$, and comment on uncertainties in quark mass ratios. We analyze estimates of the light-quark densities made over the past decade using lattice calculations and/or phenomenological inputs. We find an uncertainty in the combination $\langle N | \bar{u}u + \bar{d}d | N \rangle$ that is larger than has been assumed in some phenomenological analyses, and a range of $\langle N | \bar{s}s | N \rangle$ that is smaller but compatible with earlier estimates. We also analyze the importance of the $\mathcal{O}(\alpha_s^3)$ calculations of the heavy-quark matrix elements that are now available, which provide an important refinement of the calculation of the spin-independent scattering cross section. We use for illustration a benchmark CMSSM point in the focus-point region that is compatible with the limits from LHC and other searches.

1 Introduction

Direct searches for the scattering of weakly-interacting massive particle (WIMP) dark matter [1] are proceeding apace, with regular increases in the experimental sensitivity [2–4] and plans for new experiments capable of probing spin-independent scattering cross-sections σ_{SI}^p approaching the neutrino floor [5, 6]. It is important that these important experimental efforts be well served by theoretical efforts to minimize the uncertainties in calculations of event rates within specific models of WIMP dark matter. These include astrophysical uncertainties in the local density and velocity dis-

tribution of the WIMPs, uncertainties in the accuracy with which effective interaction operator coefficients can be calculated within a specific model, uncertainties in the matrix elements of these operators in hadronic targets, and uncertainties in nuclear structure effects. The focus of this paper is on the uncertainties in the matrix elements for scattering on nucleon targets.

There are classes of two dimension-6 four-fermion interactions that yield velocity-independent cross-sections for elastic WIMP-nucleon scattering, namely [7–9]

$$\mathcal{L} = \sum_i \alpha_{3i} \bar{\chi} \chi \bar{q}_i q_i + \sum_i \alpha_{2i} \bar{\chi} \gamma_\mu \gamma_5 \chi \bar{q}_i \gamma^\mu \gamma_5 q_i, \quad (1)$$

where the sums are over the quark flavours i . Rates for the first set of interactions $\propto \alpha_{3i}$ are related to quark contributions to the nucleon mass: $m_{q_i} \langle N | \bar{q}_i q_i | N \rangle$ and are independent of the nuclear spin, whereas rates for interactions $\propto \alpha_{2i}$ are related to nucleonic matrix elements of axial currents in nucleons: $\langle N | \bar{q}_i \gamma_\mu \gamma_5 q_i | N \rangle$, which are related to quark contributions to the nucleon spin. We discuss here the uncertainties in the matrix elements of the spin-independent interactions $\propto \alpha_{3i}$, which are relatively important, as we shall see. The uncertainties in the spin-dependent interaction matrix elements $\propto \alpha_{2i}$ are relatively small, as we discuss briefly towards the end of this paper.

Several approaches have been taken to estimating the $\langle N | \bar{q}_i q_i | N \rangle$ matrix elements. One of the first was to use octet baryon mass differences and SU(3) symmetry to estimate the combination $\sigma_0 \equiv \frac{1}{2}(m_u + m_d) \langle N | \bar{u}u + \bar{d}d - 2\bar{s}s | N \rangle$, together with data on low-energy πN scattering to estimate the quantity $\Sigma_{\pi N} \equiv \frac{1}{2}(m_u + m_d) \langle N | \bar{u}u + \bar{d}d | N \rangle$.¹ As has been discussed in previous work, see, e.g., [9, 12–15], com-

^a e-mail: olive@physics.umn.edu

¹ This quantity has also been estimated using data on pionic atoms [10, 11], with similar results, as we discuss later.

binning these estimates of σ_0 and $\Sigma_{\pi N}$ led to relatively large estimates for $\langle N|\bar{s}s|N\rangle$, though with large uncertainties.

As we discuss below in some detail, in recent years a large effort has been put into lattice calculations, which have yielded a range of values of $\Sigma_{\pi N}$ and relatively small estimates for $\langle N|\bar{s}s|N\rangle$. The corresponding values of σ_0 may be similar to the estimates made using baryon masses and SU(3), but some calculations correspond to significantly larger values of σ_0 . In parallel, there have been calculations using baryon chiral perturbation theory (B χ PT) that may lead to much larger values of σ_0 , see, e.g., [16], close to the data-based estimates of $\Sigma_{\pi N}$, which may also correspond to relatively small values of $\langle N|\bar{s}s|N\rangle$.

In this paper we compile the lattice and other estimates of $\Sigma_{\pi N}$ and $\sigma_s \equiv m_s \langle N|\bar{s}s|N\rangle$ that have appeared over the past decade, and propose simple Gaussian representations of their values and uncertainties. These may be useful for analyses of the constraints that direct searches for dark matter via spin-independent scattering impose on specific models. Our combined estimate of $\Sigma_{\pi N}$ is similar to values suggested previously, but with a larger uncertainty, while our combined estimate of σ_s is somewhat smaller than older estimates, though consistent with their uncertainties. We illustrate the results of our analysis with calculations of the spin-independent dark matter scattering cross section σ_{SI}^p at a specific benchmark point in the focus-point region [17–20] of the constrained minimal supersymmetric Standard Model (CMSSM) [21–30], noting that other supersymmetric parameter sets exhibit similar trends. As we discuss, the uncertainties in σ_{SI}^p related to light quark masses and $\langle N|\bar{u}u|N\rangle/\langle N|\bar{d}d|N\rangle$ are significantly smaller than those associated with σ_s . We also discuss the uncertainties in σ_{SI}^p associated with the heavy quark matrix elements $\langle N|\bar{c}c, \bar{b}b, \bar{t}t|N\rangle$. The b and t quarks are sufficiently heavy that a perturbative treatment of their hadronic matrix elements is appropriate, but this is not so evident for the c quark. Some lattice and other numerical estimates of $\sigma_c \equiv m_c \langle N|\bar{c}c|N\rangle$ are available, and span a wide range that straddles the perturbative estimate. If the $\mathcal{O}(\alpha_s^3)$ perturbative estimates are used for all the heavy-quark matrix elements, as we advocate, the corresponding uncertainties in σ_{SI}^p are small, but if the full range of numerical estimates of σ_c is considered the associated uncertainty is comparable to that associated with σ_s .

The layout of this paper is as follows. In Sect. 2 we review the strong-interaction quantities entering the calculation of the spin-independent cross-section σ_{SI}^p . Inputs to the calculation of σ_{SI}^p are discussed in Sect. 2.1, the individual uncertainties in the matrix elements of the densities of the light quarks u, d, s are discussed in Sect. 2.2, and their propagation into the calculation of σ_{SI}^p are discussed in Sect. 2.3. Section 2.4 is dedicated to a discussion of the matrix elements of the heavy quarks c, b, t . Finally, Sect. 3 contains a brief discussion of the uncertainties in the calculation of the

spin-dependent cross-section σ_{SD} , and our conclusions are summarized in Sect. 4.

2 Spin-independent WIMP-nucleon scattering

2.1 Inputs to the matrix element calculation

At zero momentum transfer, and neglecting nuclear structure effects, the spin-independent cross-section for the elastic scattering of a generic WIMP on a nucleus with charge Z and atomic number A can be written as [1, 7, 8, 31–39]

$$\sigma_{SI}^{Z,A} = \frac{4m_r^2}{\pi} [Zf_p + (A - Z)f_n]^2, \quad (2)$$

where m_r is the reduced WIMP mass,

$$\frac{f_N}{m_N} = \sum_q f_{T_q}^N \frac{\alpha_{3q}}{m_q} \quad (3)$$

for $N = p$ or n , and the quantities $f_{T_q}^N$ are defined by

$$m_N f_{T_q}^N \equiv \langle N|m_q \bar{q}q|N\rangle \equiv \sigma_q \equiv m_q B_q^N. \quad (4)$$

We recall that the quantities $f_{T_q}^N$ (σ_q) are independent of renormalization scheme and scale, whereas the quantities m_q and B_q^N appearing have cancelling scheme and scale dependences.

The contributions of the heavy quarks $q = c, b, t$ have often been treated by integrating them out and replacing them by the one-loop contributions due to scattering off gluons [40, 41], so that

$$\frac{f_N}{m_N} = \sum_{q=u,d,s} f_{T_q}^N \frac{\alpha_{3q}}{m_q} + \frac{2}{27} f_{T_G}^N \sum_{q=c,b,t} \frac{\alpha_{3q}}{m_q}, \quad (5)$$

where

$$f_{T_G}^N = 1 - \sum_{q=u,d,s} f_{T_q}^N. \quad (6)$$

In our subsequent analysis, this is the first approach we use to calculate $\sigma_{SI}^{p,n}$.

However, as discussed later in more detail, there are by now a number of lattice calculations of $f_{T_c}^N = m_c \langle N|\bar{c}c|N\rangle/m_N = \sigma_c/m_N$, so for comparison we also estimate σ_{SI}^p using the one-loop 4-flavour versions of (5) and (6), where

$$\sum_{q=u,d,s} \rightarrow \sum_{q=u,d,s,c}, \quad \sum_{q=c,b,t} \rightarrow \sum_{q=b,t}, \quad \frac{2}{27} \rightarrow \frac{2}{25}, \quad (7)$$

together with a numerical estimate of $f_{T_c}^N$ that is based (mainly) on lattice calculations.

As we also discuss later, there are also calculations of $f_{T_c}^N, f_{T_b}^N$ and $f_{T_t}^N$ to $\mathcal{O}(\alpha_s^3)$ in perturbative QCD. These perturbative calculations are expected to be very reliable for $f_{T_b}^N$

and $f_{T_1}^N$, perhaps less so for $f_{T_c}^N$. Therefore, we also estimate σ_{SI}^p using these calculations in the full six-flavour formula (3), for comparison with the three-quark formula (5) and the four-quark formula (7) evaluated using the available numerical estimates of $f_{T_c}^N$. As we discuss later, we consider the $\mathcal{O}(\alpha_s^3)$ six-flavour approach to be the best available at the present time.

In order to evaluate (5) we need estimates of the matrix elements $\langle N | \bar{u}u, \bar{d}d, \bar{s}s | N \rangle$, for which isospin invariance ensures that $\langle p | \bar{u}u | p \rangle = \langle n | \bar{d}d | n \rangle = B_u^p$, $\langle p | \bar{d}d | p \rangle = \langle n | \bar{u}u | n \rangle = B_d^p$ and $\langle p | \bar{s}s | p \rangle = \langle n | \bar{s}s | n \rangle = B_s^p$. An expression for one combination of these quantities is provided by the pion-nucleon σ term

$$\Sigma_{\pi N} = \frac{1}{2}(m_u + m_d)(B_u^p + B_d^p), \quad (8)$$

which may be extracted phenomenologically from data on low-energy π -nucleon scattering or on pionic atoms [10, 11]. In order to determine B_s^p , (8) has often been used in combination with the quantity

$$\sigma_0 = \frac{1}{2}(m_u + m_d)(B_u^p + B_d^p - 2B_s^p), \quad (9)$$

which can be extracted phenomenologically from the octet baryon mass splittings, taking into account corrections that can be calculated in baryonic chiral perturbation theory (B χ PT). One then has

$$\sigma_s = m_s B_s^p = \frac{m_s}{m_u + m_d}(\Sigma_{\pi N} - \sigma_0), \quad (10)$$

which is often parameterized by

$$y = 1 - \frac{\sigma_0}{\Sigma_{\pi N}} = \frac{2B_s^p}{B_u^p + B_d^p}. \quad (11)$$

However, alternatives to these phenomenological estimates are now provided by the many lattice calculations that are now available, as we discuss in Sect. 2.2 below.

In order to evaluate $\Sigma_{\pi N}$, we also need values for the ratios of quark masses m_u/m_d and m_s/m_d . In the past [15, 42], we have used the estimates

$$\frac{m_u}{m_d} = 0.553(43), \quad \frac{m_s}{m_d} = 18.9(8) \quad (12)$$

from [43], whereas the Particle Data Group (PDG) now quotes the following lattice estimates [44]:

$$\frac{m_u}{m_d} = 0.46(5), \quad \frac{2m_s}{m_u + m_d} = 27.5(3), \rightarrow \frac{m_s}{m_d} = 20.1(8). \quad (13)$$

The PDG lattice review also quotes the following absolute values of the light quark masses in the $\overline{\text{MS}}$ scheme at a renormalization scale of 2 GeV:

$$m_u = 2.15(15) \text{ MeV}, \quad m_d = 4.70(20) \text{ MeV}, \\ m_s = 93.5 \pm 2 \text{ MeV}. \quad (14)$$

In contrast, in its Summary Tables the PDG quotes the broader ranges [44]

$$\frac{m_u}{m_d} = 0.38 \text{ to } 0.58, \quad \frac{2m_s}{m_u + m_d} = 27.3(7), \\ \frac{m_s}{m_d} = 17 \text{ to } 22 \quad (15)$$

and

$$m_u = 2.2_{-0.4}^{+0.6} \text{ MeV}, \quad m_d = 4.7_{-0.4}^{+0.5} \text{ MeV}, \\ m_s = 96_{-4}^{+8} \text{ MeV}. \quad (16)$$

As we discuss below, the resulting elastic scattering cross sections we study are relatively insensitive to the values of the quark mass ratios and are completely insensitive to the absolute value of the quark mass (e.g. m_d). For definiteness, we use (14) for the value of the strange quark mass and (13) for the values of the quark mass ratios.

The quantities $B_u + B_d$ and B_s discussed above suffice to calculate the matrix elements for scattering off nuclei with equal numbers of protons and neutrons, but additional information is required to calculate the difference between the cross sections for scattering off protons and neutrons, or for the scattering off nuclei with general values of (A, Z) , as seen in (2).

Another combination of the B_q^p was calculated [45] using octet baryon masses in the relation:

$$z \equiv \frac{B_u^p - B_s^p}{B_d^p - B_s^p} = \frac{m_{\Xi^0} + m_{\Xi^-} - m_p - m_n}{m_{\Sigma^+} + m_{\Sigma^-} - m_p - m_n} = 1.49. \quad (17)$$

The uncertainty associated with measurements of the octet baryon masses is very small, but the accuracy of the octet mass formula (17) is subject to question [46, 47].

Alternatively, one can calculate z from the ratio

$$z = \frac{2 - (1 + \frac{B_d^p}{B_u^p})y}{(2 - y)\frac{B_d^p}{B_u^p} - y} \quad (18)$$

once B_u^p/B_d^p and the value of y are known. For example, the ratio B_u^p/B_d^p can be calculated from the QCD contribution to the proton-neutron mass difference:

$$m_p - m_n|_{QCD} = (m_u - m_d)(B_u^p - B_d^p), \quad (19)$$

in combination with (8):

$$\left(\frac{m_u}{m_d} - 1\right) \left(1 - \frac{B_d^p}{B_u^p}\right) = \frac{(m_p - m_n)|_{QCD}}{2\Sigma_{\pi N}}, \quad (20)$$

using the value (13) of m_u/m_d . The measured mass difference $m_p - m_n = -1.29$ MeV (with negligible uncertainty) and the electromagnetic contribution is estimated to be $m_p - m_n|_{QED} = 1.04(11)$ MeV [48], leading to

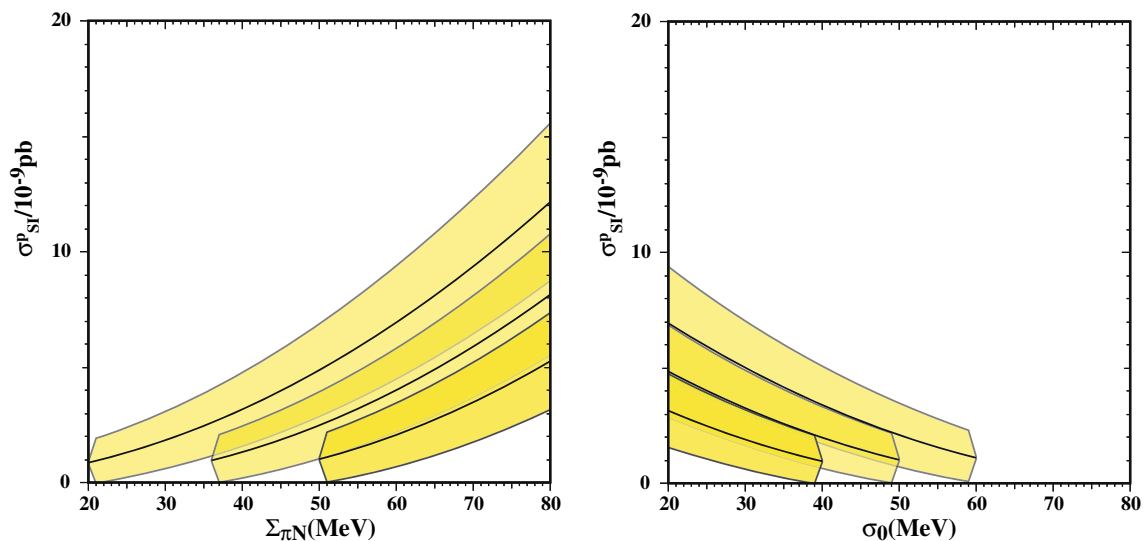


Fig. 1 Left: σ_{SI}^p vs $\Sigma_{\pi N}$ for $\sigma_0 = 20, 36, 50$ MeV. Right: σ_{SI}^p vs σ_0 for $\Sigma_{\pi N} = 40, 50, 60$ MeV. The color bands show the $1\text{-}\sigma$ uncertainty in the elastic cross section calculated using the three-flavour expression (5)

$m_p - m_n|_{QCD} = -2.33(11)$ MeV. Inserting the central value of m_u/m_d from (13) and the central value of $\Sigma_{\pi N}$ from (24) below into (20) to evaluate B_d^p/B_u^p , and then using (18) with y given by the central values of $\Sigma_{\pi N}$ and σ_s in (24) and (25) below, respectively, we estimate

$$z = 1.16. \quad (21)$$

A similar value $z = 1.258(81)$ was found independently in a lattice calculation in [49]. Conservatively, we consider the range $1 < z < 2$ in our subsequent estimates.

2.2 Uncertainties in $\Sigma_{\pi N}$, σ_0 and σ_s

The most important uncertainties in calculations of the spin-independent WIMP-nuclear scattering matrix elements are those in $\Sigma_{\pi N}$ and σ_s . In the past, σ_s has often been evaluated by combining phenomenological estimates of $\Sigma_{\pi N}$ (8) and σ_0 (9) using (10). The uncertainties in $\Sigma_{\pi N}$ and σ_0 translate into significant uncertainties in the spin-independent cross section [9, 12–15],² as illustrated in Fig. 1, where the three-flavour expression (5) has been used. Here and in the analysis that follows, we use a representative point in the CMSSM consistent with the limits from LHC and other searches [30], namely with $m_{1/2} = 3000$ GeV, $m_0 = 8200$ GeV, $A_0 = 0$ GeV, $\tan \beta = 10$, and $\mu > 0$. At this point, the LSP is mainly a Higgsino with mass $\simeq 1.1$ TeV whose relic density matches that determined by CMB experiments [50, 51]. We have verified that similar trends in the dependences on $\Sigma_{\pi N}$ and σ_0 arise at other representative points, namely a stop-coannihilation point and s-channel A/H funnel point, though

the values of the elastic cross section is very different for these points.

The left panel of Fig. 1 shows the values of σ_{SI}^p obtained as a function of $\Sigma_{\pi N}$ for three indicative values of $\sigma_0 = 20, 36, 50$ MeV, and the right panel of Fig. 1 shows the values of σ_{SI}^p obtained as a function of σ_0 for the three indicative values $\Sigma_{\pi N} = 40, 50, 60$ MeV. In the two cases, representative uncertainties of 7 MeV were assumed in σ_0 and $\Sigma_{\pi N}$, respectively. In making these plots, we have assumed that $B_s \geq 0$ and hence imposed the restriction $\Sigma_{\pi N} \geq \sigma_0$. For the indicative values $\Sigma_{\pi N} = 50 \pm 7$ MeV and $\sigma_0 = 36 \pm 7$ MeV, we find $\sigma_{SI}^p = (2.5 \pm 1.5) \times 10^{-9}$ pb using the three-flavour formula (5).

‘Legacy’ values of $\Sigma_{\pi N}$ and σ_0 quoted in [15] were $\Sigma_{\pi N} = 64(8)$ MeV from π -N scattering and $\sigma_0 = 36(7)$ MeV from octet baryon mass differences [52–56]. Subsequently, since lattice calculations have tended to yield lower values of $\Sigma_{\pi N} \gtrsim 40$ MeV, and the MasterCode collaboration has been using the ‘compromise’ value $\Sigma_{\pi N} = 50(7)$ MeV when using the experimental limits on spin-independent dark matter scattering on nuclei in global fits to supersymmetric models (see, e.g., [42]). In combination with $\sigma_0 = 36(7)$ MeV [52–56], this yields $\sigma_s = 192(136)$ MeV. Another global fitting group, the GAMBIT Collaboration (see, e.g., [57]), has, on the other hand, been using the smaller value $\sigma_s = 43(8)$ MeV, which is based on a compilation of lattice data made in 2011 [58], together with a larger value of $\Sigma_{\pi N} = 58(9)$ MeV. This combination corresponds to $\sigma_0 = 55$ MeV, considerably larger than the estimate from octet baryon mass differences [52], but within the range argued in [16] to be consistent with B χ PT.

² We describe the propagation of these uncertainties in Sect. 2.3.

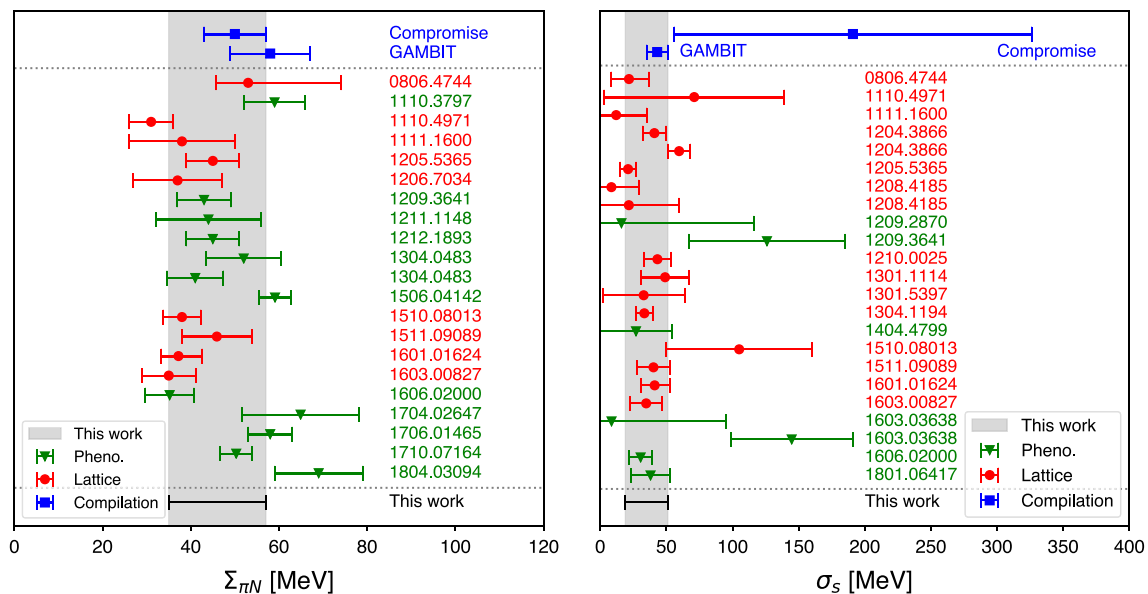


Fig. 2 Left panel: Recent values of $\Sigma_{\pi N}$. Right panel: Recent values of σ_s . Calculations based mainly on lattice calculations are indicated in red, and those relying more on phenomenological inputs are indicated

Here we revisit the uncertainties in $\Sigma_{\pi N}$ and σ_s based on the considerable effort during the last decade made since [15], using lattice and other techniques, to determine $\Sigma_{\pi N}$ and σ_s [59]. Although most of these recent values have been obtained from lattice calculations, many have been based on the phenomenology of low-energy π -nucleon interactions, and some have made extensive use of chiral perturbation theory, often in combination with lattice techniques. As already commented in [60], and discussed in more detail below, there is tension between these various estimates, and the uncertainties are not purely statistical.

The left panel of Fig. 2 displays all the estimates of $\Sigma_{\pi N}$ that we use, and the right panel displays all the estimates of σ_s that are included in our analysis. We have tried to make a complete selection of all the determinations of these quantities that have not been superseded by later analyses by strongly-overlapping research groups. In each case, we have indicated by colour coding the primary phenomenological technique used in the calculation, and we have also indicated the corresponding arXiv reference number. We also indicate by shaded bands in Fig. 2 the estimates of $\Sigma_{\pi N}$ and σ_s that we make on the basis of this new compilation, using the prescription that we describe below. More details of the determinations we use, including their numerical values, are given in Table 1.³

We now discuss the combinations of these estimates using the procedures adopted by the Particle Data Group (PDG) in cases where the uncertainties are not simply statistical

in green. We also show the estimates made in previous compilations [42, 57] (blue), and the values we estimate now on the basis of our new compilation (bottom line and vertical grey bands)

[44]. Assuming uncorrelated Gaussian probability distributions for each of the estimates of $\Sigma_{\pi N}$ shown in the left panel of Fig. 2, we first construct the ideogram⁴ shown in the left panel of Fig. 3. As can be discerned from Fig. 2, the values of $\Sigma_{\pi N}$ are broadly distributed between 40 and 60 MeV, and the ideogram exhibits 3 minor peaks, slightly favoring the lower part of the range.

A naive weighted mean of all 21 determinations of $\Sigma_{\pi N}$ yields

$$\text{Naive: } \Sigma_{\pi N} = 46.1 \pm 1.3 \text{ MeV}, \quad (22)$$

where we have combined statistical and systematic uncertainties in quadrature and centred asymmetric errors. It is clear, however, that this naive estimate would be a poor representation of the ideogram. One option proposed by the PDG under such circumstances is to rescale the error so that the $\chi^2/\text{d.o.f.} = 1$. In this case, the required renormalization factor is 1.7, yielding

$$\text{Rescaled: } \Sigma_{\pi N} = 46.1 \pm 2.2 \text{ MeV}. \quad (23)$$

However, this would also be a poor representation of the ideogram, in view of its serrated ridge top that is broader than the rescaled distribution (23).⁵ The rescaled value is

³ We apologize in advance to authors whose work we have overlooked or misrepresented in compiling this Table, and welcome suggestions for its completion and improvement.

⁴ The ideogram is constructed using the prescription of the PDG [44], and is a sum of Gaussians for each measurement with an area normalized to be $1/\sigma_i$ where σ_i is the uncertainty in the measurement.

⁵ This feature may reflect the existence of unidentified systematic uncertainties that affect different lattice methods and B χ PT approaches in different ways.

Table 1 Estimates of $\Sigma_{\pi N}$ and σ_s

References	$\Sigma_{\pi N}$	Uncertainties	σ_s	Uncertainties	Method
[42]	50	7	191	135	Compilation
[57]	58	9	43	8	Compilation
[61]	53	2^{+21}_{-7}	21.7	$^{+15.1}_{-13.4}$	Lattice
[62]	59	7			B χ PT, π atoms
[63]	31	3 ± 4	71	34 ± 59	Lattice
[64]	38	12	12	$^{+23}_{-16}$	Lattice
[65]			40.9	7.5 ± 4.7	Lattice
			59.6	5.1 ± 6.9	Lattice
[66]	45	6	21	6	Lattice
[67]	37	8 ± 6			Lattice
[68]			8.4	14.1 ± 15.0	Lattice
			21.6	27.2 ± 26.3	Lattice
[16]			16	80 ± 60	B χ PT
[69]	43	1 ± 6	126	24 ± 54	Lattice/B χ PT
[70]			43.2	10.3	Lattice
[71]	44	12			πN scattering
[72]	45	6			πN scattering
[73]			49	10 ± 15	Lattice
[74]			32.8	31.0	Lattice
[75]	52	3 ± 8			Lattice/B χ PT
	41	5 ± 4			Lattice/B χ PT
[76]			33.3	6.2	Lattice/B χ PT
[77]			27	27 ± 4	Lattice/B χ PT
[78, 79]	59.1	1.9 ± 3			π atoms
[80]	38	3 ± 3	105	41 ± 37	Lattice
[81]	45.9	7.4 ± 2.8	40.2	11.7 ± 3.5	Lattice
[82]	37.2	$2.6^{+4.7}_{-2.9}$	41.1	$8.2^{+7.8}_{-5.8}$	Lattice
[49]	35	6.1	34.7	12.2	Lattice
[83]			8.5	4.4 ± 86.6	π atoms, πN scattering
			144.7	4.6 ± 45.9	π atoms, πN scattering
[84]	35.2	5.5	30.5	8.5	B χ PT
[85]	64.9	1.5 ± 13.2			Lattice/B χ PT
[86]	58	5			πN scattering
[87]	50.3	1.2 ± 3.4			Lattice/B χ PT
[88, 89]	48		38	15	Lattice/B χ PT
[90]	69	10			B χ PT
This work	46	11	35	16	New compilation

Estimates of $\Sigma_{\pi N}$ and σ_s (in MeV units). The first two lines are from previous compilations. The following lines are from recent determinations and, where two errors are quoted, the first is statistical and the second systematic. As indicated, most of the determinations are based on lattice calculations, many use baryon chiral perturbation theory (B χ PT), three use data on pionic atoms (π atoms) and five use low-energy πN scattering data. The last line is our new compilation

displayed in the left panel of Fig. 3 as a vertical pink bar, for comparison with the ideogram.

As an alternative, we present in the right panel of Fig. 3 a representation of the estimates as a single Gaussian with the same normalization as the ideogram, and with its central

value and error chosen to reproduce the 95% CL range of the ideogram as closely as possible:

$$\text{Gaussian representation: } \Sigma_{\pi N} = 46 \pm 11 \text{ MeV.} \quad (24)$$

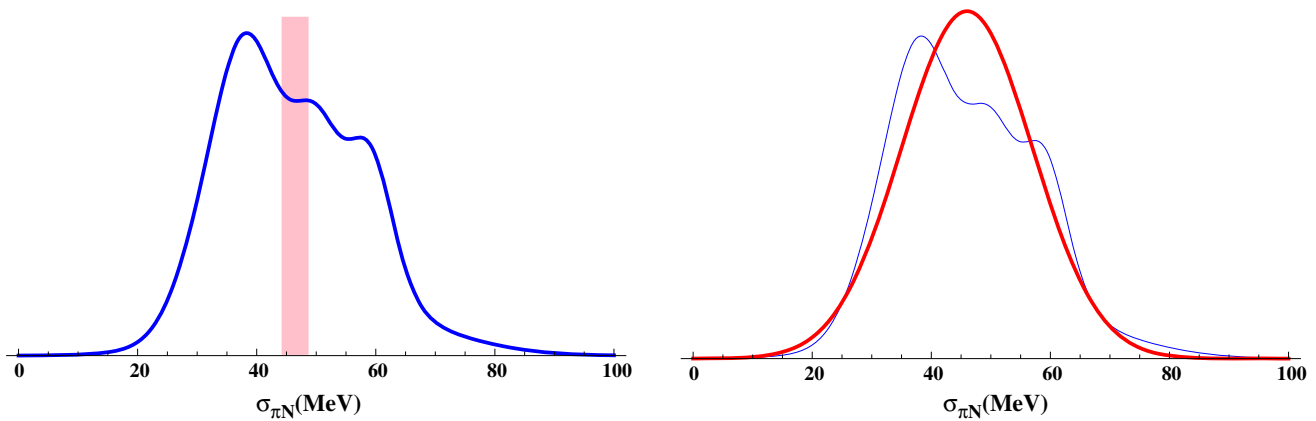


Fig. 3 Left panel: Ideogram combining all values of $\Sigma_{\pi N}$ from Table 1. The vertical (pink) bar corresponds to the estimate (23). Right panel: The same ideogram compared with a (red) Gaussian centred at $\Sigma_{\pi N} = 46$ MeV with error $\sigma = 11$ MeV

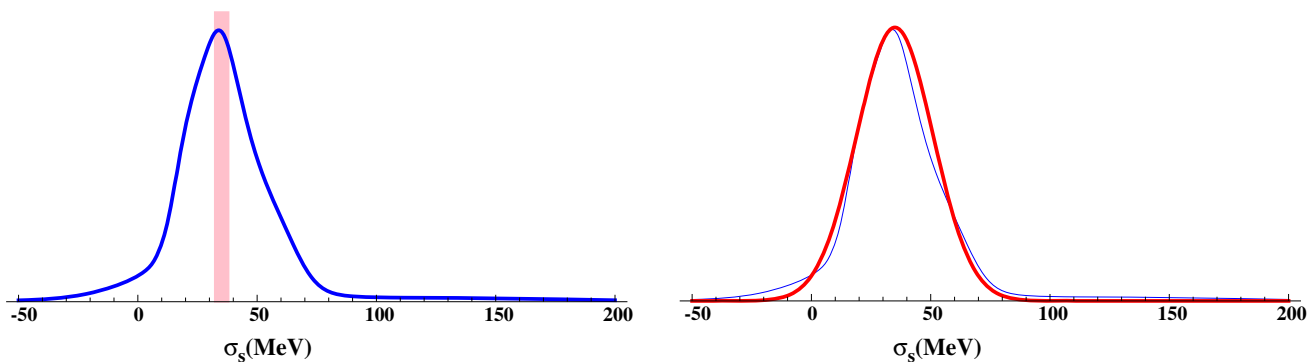


Fig. 4 Left panel: Ideogram combining all values of σ_s . Right panel: Ideogram combining all values of σ_s compared with a Gaussian centred at $\sigma_s = 35$ MeV with width $\sigma = 16$ MeV

Although this functional form is far from perfect, we consider it a simple but fair representation of current estimates of $\Sigma_{\pi N}$.

Figure 4 shows the result of a similar exercise for the 23 determinations of σ_s that we use. In this case the ideogram has (barely) visible support out to very large values, but most of the numerical values have support only for $\sigma_s < 100$ MeV. Following the same steps as used previously for $\Sigma_{\pi N}$, we find

$$\begin{aligned} \text{Naive:} \quad & \sigma_s = 35.2 \pm 2.6 \text{ MeV}, \\ \text{Rescaled:} \quad & \sigma_s = 35.2 \pm 3.1 \text{ MeV}, \\ \text{Gaussian representation:} \quad & \sigma_s = 35 \pm 16 \text{ MeV}. \end{aligned} \quad (25)$$

In this case the distribution obtained from the numerical estimates is again not symmetric, though it has a single-peak structure, and the representation (25) may again be considered a simple but fair representation of current estimates of σ_s .

2.3 Uncertainties in the elastic scattering cross-section

We now discuss the combination of the uncertainties in $\Sigma_{\pi N}$ and σ_s in the calculation of σ_{SI}^p . A scatter plot of values of $(\Sigma_{\pi N}, \sigma_s)$ from references in which values of both quantities

are quoted (see Table 1) is shown in the left panel of Fig. 5. The horizontal and vertical grey bands show the ranges of $\Sigma_{\pi N}$ and σ_s that we estimate on the basis of our global analysis. The right panel of Fig. 5 displays a two-dimensional joint ideogram of $\Sigma_{\pi N}$ and σ_s based on the determinations in Fig. 5. We have studied via a regression analysis whether these determinations exhibit any correlations between $\Sigma_{\pi N}$ and σ_s . We find a slope in the $(\Sigma_{\pi N}, \sigma_s)$ plane of 0.49 ± 1.08 , i.e., no significant correlation. In the rest of this analysis we assume that there is no correlation between the uncertainties in $\Sigma_{\pi N}$ and σ_s .

The analogue of Fig. 1 in terms of $\Sigma_{\pi N}$ and σ_s is shown in Fig. 6, where the values of σ_{SI}^p are again calculated using the three-flavour expression (5). In the left panel, we see that for fixed σ_s , there is no longer the large dependence of the cross section on $\Sigma_{\pi N}$ that was seen in Fig. 1. The three bands (which overlap) correspond to $\sigma_s = 30, 50$ and 100 MeV. In the right panel, there are three bands corresponding to fixed values of $\Sigma_{\pi N} = 40, 50$ and 60 MeV that lie almost on top of each other, and one sees quite clearly the dependence of the cross section on σ_s . Note that the thickness of the bands here are significantly narrower than those in Fig. 1. This is

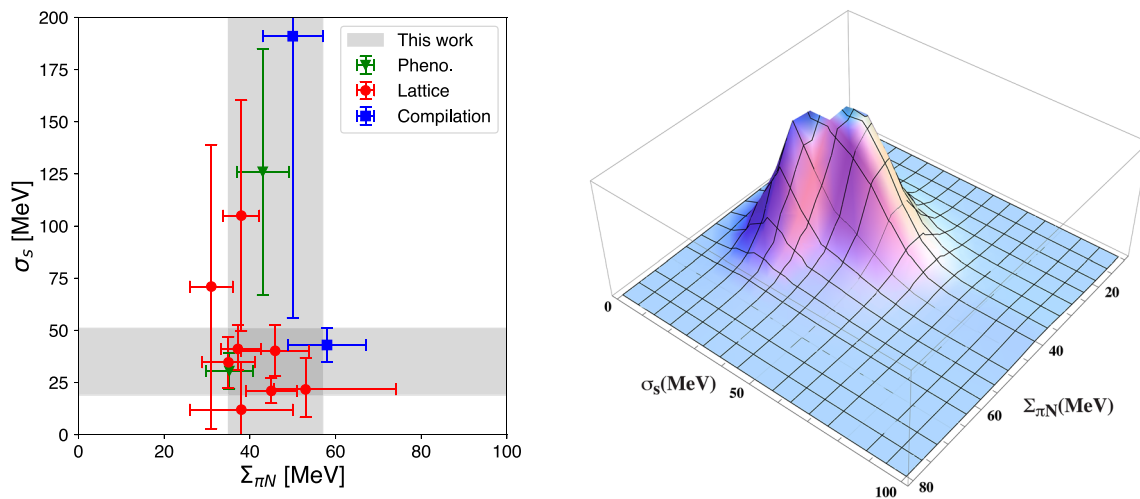


Fig. 5 Scatter plot of $(\Sigma_{\pi N}, \sigma_s)$, with grey bands showing the ranges of $\Sigma_{\pi N}$ and σ_s that we estimate on the basis of our new compilation. Right panel: Two-dimensional ideogram of $\Sigma_{\pi N}$ and σ_s

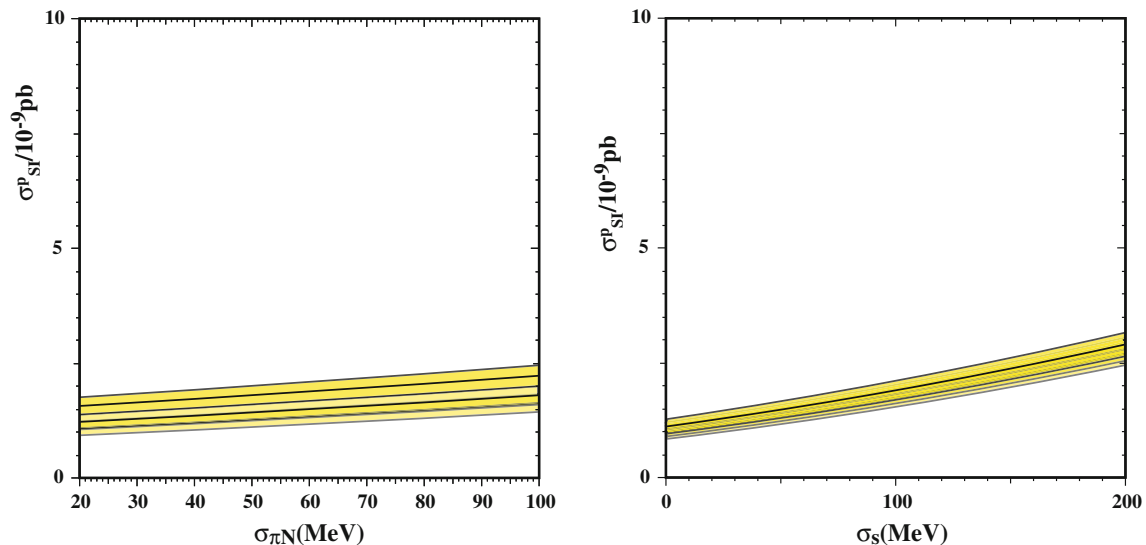


Fig. 6 Left: σ_{SI}^p vs $\Sigma_{\pi N}$ for $\sigma_s = 30, 50, 100$ MeV. Right: σ_{SI}^p vs σ_s for $\Sigma_{\pi N} = 40, 50, 60$ MeV. The color bands show the calculated 1 σ uncertainty in the elastic cross section

mainly due to the smaller uncertainty in σ_s when it is taken directly from Eq. (25) rather than derived indirectly using estimates of σ_0 . Using σ_s as an input into calculations of $\Sigma_{\pi N}$ is therefore preferred.

We now show how the uncertainties in $\Sigma_{\pi N}$ and σ_s discussed above can be propagated into the uncertainty in the elastic scattering cross section. As we have discussed, the distributions for the hadronic matrix elements are not Gaussian, but we have provided Gaussian approximations to those distributions in (24) and (25), which we propagate to the errors in the cross section. We describe our procedure for scattering on protons only, the neutron case being simply related by an isospin transformation.

The uncertainty in the elastic cross section on a proton is simply

$$\sigma_{\sigma_{SI}^p} = 2\sigma_{SI}^p \frac{\sigma_{f_p}}{f_p}, \quad (26)$$

where

$$\sigma_{f_p} = m_p \left(\sum_{q=u,d,s} \sigma_{f_{Tq}^p}^2 \left[(\alpha_{3q}/m_q) - \frac{2}{27} \left(\sum_{q=c,b,t} \alpha_{3q}/m_q \right) \right]^2 \right)^{1/2}. \quad (27)$$

Since we are using σ_s and its uncertainty directly, calculating the uncertainty in $f_{T_s}^p = \sigma_s/m_p$ is straightforward:

$$\sigma_{f_{T_s}^p} = f_{T_s}^p \frac{\sigma_{\sigma_s}}{\sigma_s}. \quad (28)$$

In the cases of the other light quarks, the expressions for $f_{T_q}^p$ are more complicated:

$$\begin{aligned}
 m_p f_{T_u}^p &= \frac{2\Sigma_{\pi N}}{(1 + \frac{m_d}{m_u})(1 + \frac{B_d^p}{B_u^p})} \\
 &= \frac{2m_u}{m_u + m_d} \left[\frac{z}{1+z} \Sigma_{\pi N} + \frac{m_u + m_d}{2m_s} \frac{1-z}{1+z} \sigma_s \right] \\
 m_p f_{T_d}^p &= \frac{2\Sigma_{\pi N}}{(1 + \frac{m_u}{m_d})(1 + \frac{B_d^p}{B_u^p})} \\
 &= \frac{2m_d}{m_u + m_d} \left[\frac{1}{1+z} \Sigma_{\pi N} - \frac{m_u + m_d}{2m_s} \frac{1-z}{1+z} \sigma_s \right],
 \end{aligned} \quad (29)$$

where the right-hand sides of the equations allow us to compute the $f_{T_q}^p$ directly from our inputs. To obtain the uncertainties in $f_{T_{u,d}}^p$, we propagate the uncertainties in $\Sigma_{\pi N}$, the light quark mass ratio $m_u/m_d = 0.46 \pm 0.05$ (13), and in the ratio B_d/B_u given in Eq. (18). This depends on the uncertainty in y , and hence depends ultimately on the uncertainties in $m_s/(m_u + m_d) = 13.75 \pm 0.15$ and σ_s . The expression (27) takes into account the correlation in the uncertainties between the light and heavy quark contributions.

We have verified in the benchmark model assumed that the uncertainties in m_u/m_d and in m_s/m_d given in (14) contribute very small uncertainties to σ_{SI}^p , a few per mille and below one per mille respectively. The uncertainty due to B_d^p/B_u^p is also small, at the $\pm 2\%$ level for $1 < z < 2$.⁶ We note that our benchmark point is taken from a supersymmetric theory and the scattering of the dark matter candidate in this model on a proton is dominated by the heavy quark content. It is quite possible that other dark matter candidates are more sensitive to the scattering off of light quarks and in that case, the uncertainty due to B_d^p/B_u^p and z is more important.

We display in Fig. 7 contours of σ_{SI}^p (in units of 10^{-9} pb) in the $(\Sigma_{\pi N}, \sigma_s)$ plane calculated using the three-flavour expression (5), together with the two-dimensional 68% and 95% CL regions ($\Delta\chi^2 < 2.3$ and 5.99, respectively) given by our Gaussian fits (24, 25) to $\Sigma_{\pi N}$ and σ_s , assuming that there is no correlation, as discussed above.

Using our values for $\Sigma_{\pi N}$ (24) and σ_s (25) that are also given in the last line of Table 1, we find $\sigma_{SI}^p = (1.25 \pm 0.13) \times 10^{-9}$ pb when we use the three-flavour expression (5) for our CMSSM benchmark point. The decrease in the cross section (by a factor of 2) relative to what we would have calculated using the values of $\Sigma_{\pi N}$ and σ_0 used in [42] is due largely to the effective reduction in σ_s . Moreover, the uncertainty in the cross section is a factor of 10 smaller. This reduction can be traced to using σ_s (and its uncertainty) directly from the recent calculations - as we recommend - rather than using

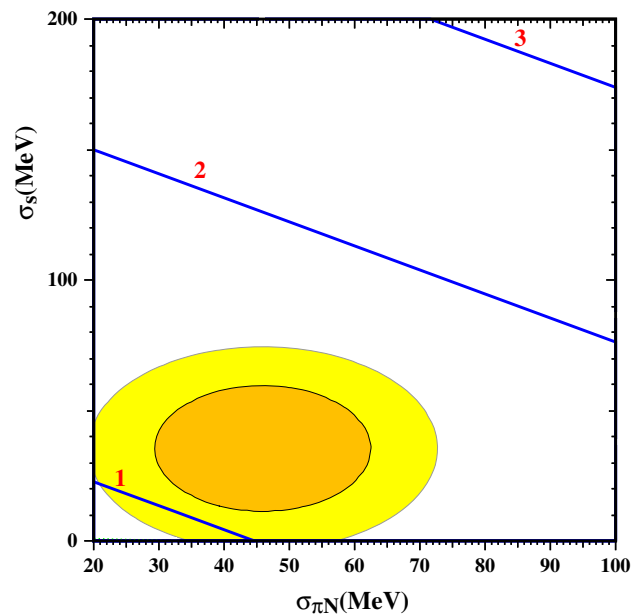


Fig. 7 Contours of σ_{SI}^p (in units of 10^{-9} pb) in the $(\Sigma_{\pi N}, \sigma_s)$ plane, with the two-dimensional 68% and 95% CL regions (darker and lighter shading) given by our Gaussian fits (24, 25) to $\Sigma_{\pi N}$ and σ_s

the value inferred from (10) and the older values of $\Sigma_{\pi N}$ and σ_0 .

2.4 Dependence on heavy quark matrix elements

In this section, we explore the sensitivity of σ_{SI}^p to the heavy quark matrix elements, using first the four-quark version (7) of the cross-section formula, and then the full six-flavour version.

There have been several calculations of the charm quark contribution to the proton mass, $\sigma_c \equiv m_c \langle N | \bar{c}c | N \rangle$, most using lattice techniques, as shown in Fig. 8 and Table 2. There have also been some phenomenological estimates of σ_c , as also shown there. We do not include in our global fit the last three estimates, which depend on particular hypotheses concerning the fraction of the proton momentum in the infinite-momentum frame that is carried by $\bar{c}c$ pairs [91]. In the absence of a clear criterion for choosing between these hypotheses, we do not use them. An ideogram of the estimates of σ_c that we retain is shown in Fig. 9. Following the same steps as used previously for $\Sigma_{\pi N}$ and σ_s , we find

$$\begin{aligned}
 \text{Naive : } \quad \sigma_c &= 50.2 \pm 8.5 \text{ MeV}, \\
 \text{Rescaled : } \quad \sigma_c &= 50.2 \pm 9.6 \text{ MeV}.
 \end{aligned}$$

However, it is clear that these are exceedingly poor representations of the ideogram shown in Fig. 9, which is highly asymmetric. We choose to represent this by summing a pair of Gaussians G , with arbitrary normalizations and the following central values and errors: the maximum:

⁶ Over this range of z , $\sigma_{SI}^p/\sigma_{SI}^n$ varies between 1.00 and 0.94.

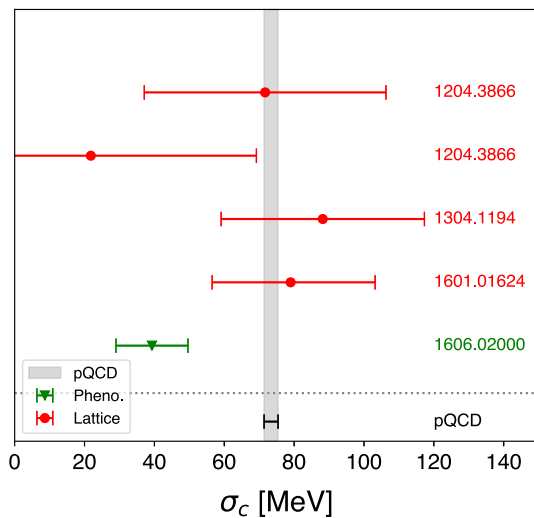


Fig. 8 Calculations of σ_c (in MeV units). Those made using the lattice are indicated in red, and one relying on phenomenological inputs is indicated in green. We also show the $\mathcal{O}(\alpha_s^3)$ perturbative calculation (33) (bottom line and vertical grey band)

Table 2 Estimates of σ_c

Reference	σ_c	Uncertainties	Method
[65]	71.7	34.6	Lattice
	21.8	47.4	Lattice
[76]	88.2	29.1	Lattice
[82]	79	21^{+12}_{-8}	Lattice
[84]	39.3	10.3	Phenomenology
[91]	4.3	4.4	Phenomenology
	12.5	13	Phenomenology
	32.3	33.6	Phenomenology

Calculations of σ_c (in MeV units). Where two errors are quoted, the first is statistical and the second systematic. As indicated, most of the determinations are based on lattice calculations. The last group of three phenomenological estimates are not included in our global fit

Gaussian representation :

$$\sigma_c = G(40 \text{ MeV}, 12 \text{ MeV}) + G(82 \text{ MeV}, 25 \text{ MeV}). \quad (30)$$

This representation is also shown in Fig. 9, and gives a very good representation of the estimates in Table 2.

Using the four-quark expression (7) and the first Gaussian for σ_c in (30), we find $\sigma_{SI}^P = (1.07 \pm 0.15) \times 10^{-9}$ pb, whereas the second Gaussian in (30) yields $\sigma_{SI}^P = (1.40 \pm 0.25) \times 10^{-9}$ pb, reflecting its larger central value and error. We note that, in the computation of these uncertainties, Eq. (27) must be modified in a way similar to Eq. (7), namely the first sum is over the four quarks u, d, s, c , $2/27 \rightarrow 2/25$, and the second sum is over two quarks b, t .

Alternatively, one could adopt the value for σ_c taken from a perturbative QCD calculation using the one-loop contribu-

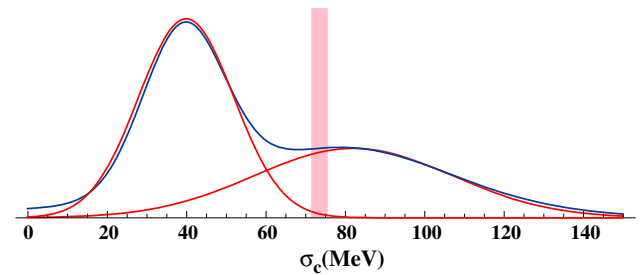


Fig. 9 Ideogram compiling lattice and phenomenological calculations of σ_c and our representation as a sum of two Gaussians (30). Also shown is a vertical pink band from our evaluation of the $\mathcal{O}(\alpha_s^3)$ perturbative QCD calculation of [92], shown in (33)

tion associated with the gluon contribution [40,41] so that⁷:

$$\sigma_c = \frac{2}{27} M_N f_{TG}^P = 69.5 f_{TG}^P. \quad (31)$$

Using our estimates (24, 25) of $\Sigma_{\pi N}$ and σ_s , we find $f_{TG}^P = 0.917 \pm 0.019$ and hence

$$\sigma_c = (63.7 \pm 1.3) \text{ MeV}, \quad (32)$$

which lies between are two Gaussian estimates of σ_c . Not surprisingly, the cross section calculated this way, $\sigma_{SI}^P = (1.25 \pm 0.14) \times 10^{-9}$ pb, is almost identical to our 3-quark calculation using $\Sigma_{\pi N}$ and σ_s . In fact, this approach does not distinguish between the contributions of the heavy quarks and would imply $\sigma_b = \sigma_t = \sigma_c$ at this order in perturbation theory. Using Eq. (32) for all 3 heavy quarks gives $\sigma_{SI}^P = (1.24 \pm 0.17) \times 10^{-9}$ pb. Figure 10 displays the sensitivity of σ_{SI}^P to the assumed value of σ_c in the four-quark formula (left panel) and $\sigma_c = \sigma_b = \sigma_t$ in the six-quark formula (right panel). In both panels we have set $\Sigma_{\pi N} = 46$ MeV, and the 3 bands correspond again to $\sigma_s = 30, 50$ and 100 MeV.

One can go beyond the above 1-loop calculation and improve the perturbative QCD calculation for σ_c by going to $\mathcal{O}(\alpha_s^3)$ [92–94]. Using Eq. (2.13) from [92] and $f_{TG}^P = 0.917 \pm 0.019$, we find

$$\sigma_c = \frac{2}{27} \left(-0.3 + 1.48 f_{TG}^P \right) m_p = 73.4 \pm 1.9 \text{ MeV}. \quad (33)$$

Also shown in Fig. 9 is a vertical pink band corresponding to this evaluation of the $\mathcal{O}(\alpha_s^3)$ perturbative QCD calculation [92]. It has been argued (see [95] for a review) that there may be non-perturbatively-generated intrinsic charm in the nucleon, in which case the perturbative calculation leading to (33) would be inapplicable. Another potential source of difference is caused by higher-dimensional operators that are

⁷ Here and in the rest of this section we give results for $\sigma_{c,b,t}$ in the proton. Because of isospin violation, perturbative calculations of the central values in the neutron yield slightly different results, but these are indistinguishable within the uncertainties. We report results for the $f_{TG,b,t}^{P,n}$ separately in Table 3 below.

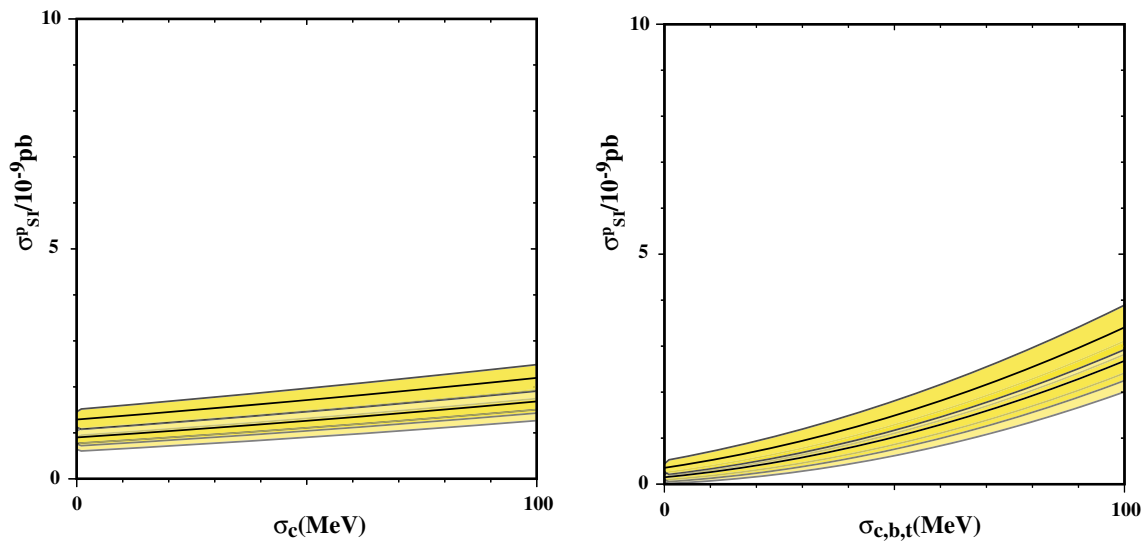


Fig. 10 Left: σ_{SI}^p vs σ_c for fixed $\Sigma_{\pi N} = 46$ MeV and $\sigma_s = 30, 50, 100$ MeV. Right: σ_{SI}^p vs $\sigma_c = \sigma_b = \sigma_t$ for fixed $\Sigma_{\pi N} = 46$ MeV and $\sigma_s = 30, 50, 100$ MeV

Table 3 Values of the $f_{T_{q,G}}^N$

Nucleon	$f_{T_u}^N$	$f_{T_d}^N$	$f_{T_s}^N$	$f_{T_G}^N$	$f_{T_c}^N$	$f_{T_b}^N$	$f_{T_t}^N$
Proton	0.018(5)	0.027(7)	0.037(17)	0.917(19)	0.078(2)	0.072(2)	0.069(1)
Neutron	0.013(3)	0.040(10)	0.037(17)	0.910(20)	0.078(2)	0.071(2)	0.068(2)

Values of the $f_{T_{q,G}}^N$ for the proton and neutron obtained using our estimates of $\Sigma_{\pi N}$ and σ_s as described in the text, assuming $z = 1.49$. The values for the heavy quarks are obtained from those for light quarks and gluons via an $\mathcal{O}(\alpha_s^3)$ calculation in perturbative QCD

induced when the charmed quark is integrated out [92], which are suppressed only by the charmed quark mass and thus may give a significant contribution to the nucleon mass. The difference between (30) and (33) may serve as a measure of the uncertainty associated with these possibilities.

Similar $\mathcal{O}(\alpha_s^3)$ perturbative QCD calculations for the b and t quarks are expected to be more reliable, and yield [92]:

$$\begin{aligned}\sigma_b &= \frac{2}{27} \left(-0.16 + 1.23 f_{T_G}^N \right) M_N, \\ \sigma_t &= \frac{2}{27} \left(-0.05 + 1.07 f_{T_G}^N \right) M_N,\end{aligned}\quad (34)$$

which, in combination with our estimates (24, 25) of $\Sigma_{\pi N}$ and σ_s , and $f_{T_G}^N$ yield

$$\sigma_b = 67.3 \pm 1.6 \text{ MeV}, \quad \sigma_t = 64.7 \pm 1.4 \text{ MeV}, \quad (35)$$

for the proton. Using the $\mathcal{O}(\alpha_s^3)$ perturbative calculations of σ_c (33) and of $\sigma_{b,t}$ (35) in a full six-flavour calculation, we find $\sigma_{SI}^p = (1.38 \pm 0.17) \times 10^{-9}$ pb. The origin of the increase from the three-flavour approximation to the full six-flavour calculation is primarily the fact that the more detailed perturbative treatment of the heavy quarks increases their contributions, particularly that of the charmed quark, by $\mathcal{O}(15)\%$.

We consider the full six-flavour calculation using the estimates (24, 25, 33) and (35) to be the best approximation

to the spin-independent WIMP scattering cross section currently available.

3 Spin-dependent WIMP-nucleon scattering

In the case of the cross section σ_{SD} for spin-dependent WIMP-nucleon scattering, the relevant matrix elements $\langle N | \bar{q}_i \gamma_\mu \gamma_5 q_i | N \rangle$ are related to the corresponding quark contributions to the nucleon spin Δq_i . The combination $\Delta u - \Delta d = g_A = 1.27$, the axial-current matrix element in neutron β -decay, which is known quite precisely. We estimate the combination $\Delta u + \Delta d - 2\Delta s = 0.59$ using other octet baryon weak decay matrix elements and SU(3) symmetry. A third combination of the light-quark Δq_i can be determined from parity-violating asymmetries in polarized deep-inelastic electron- and muon-nucleon scattering [96], which indicate a small but non-zero negative value of $\Delta s = -0.09 \pm 0.03$ when combined with the above-mentioned estimated of $\Delta u - \Delta d$ and $\Delta u + \Delta d - 2\Delta s$. Measurements of hadron production asymmetries in polarized deep-inelastic scattering do not support a non-zero value of Δs . Nevertheless, this confusion in the estimates of the Δq_i generates only moderate uncertainty in the cross section for spin-dependent WIMP-nucleon scattering, σ_{SD} .

For the CMSSM focus-point benchmark point introduced above, we find that the value $\Delta s = -0.09 \pm 0.03$ indicated by the parity-violating asymmetries in the total polarized deep-inelastic cross sections leads to $\sigma_{SD}^p = (9.4 \pm 0.8) \times 10^{-7}$ pb, whereas the choice $\Delta s = 0 \pm 0.03$ would yield $\sigma_{SD}^p = (8.2 \pm 0.7) \times 10^{-7}$ pb. The uncertainty in the spin-dependent cross section is largely determined by the uncertainty in Δs , and ignoring the uncertainty in Δs would reduce the uncertainty in σ_{SD}^p to ± 0.2 . The corresponding cross-section for scattering off neutrons is $\sigma_{SD}^p = (7.1 \pm 0.7) \times 10^{-7}$ pb for $\Delta s = -0.09$. When $\Delta s = 0$, there is virtually no difference between the cross sections for scattering on protons and neutrons. We conclude that the uncertainties in spin-dependent WIMP-nucleon scattering are comparable to the current uncertainties in spin-independent WIMP-nucleon scattering that have been the main focus of this paper.

4 Conclusions

We have re-analyzed in this paper ingredients in the calculation of the cross section for the spin-independent scattering of a massive WIMP on a nucleon. Based on available recent calculations using lattice and other techniques, we have used the prescription of the PDG to discuss the uncertainties in the quark scalar densities $\langle N|\bar{q}q|N\rangle$. We find a central value for the combination $\Sigma_{\pi N}$ of u and d densities that is somewhat smaller than found in previous compilations [15, 42, 57], though with a larger uncertainty: $\Sigma_{\pi N} = 46 \pm 11$ MeV. All determinations are compatible within the stated errors. We also find $\sigma_s = m_s \langle N|\bar{s}s|N\rangle = 35 \pm 16$ MeV, which is again smaller than suggested in previous compilations, with an uncertainty that is significantly smaller than in [15, 42] but somewhat larger than in [57]. We find (for the benchmark supersymmetric model we have studied) that the uncertainty in σ_s is the largest single source of uncertainty in σ_{SI} when it is calculated using the leading-order three-flavour approximation (5) for the spin-independent scattering matrix element.⁸ The corresponding values of the $f_{T_{u,d,s,G}}^N$ for scattering on protons and neutrons obtained assuming $z = 1.49$ are shown in the first four columns of Table 3, where we include the uncertainties due to the u, d, s mass ratios. Note that although the spin-independent cross section is not particularly sensitive to z , the values of $f_{T_{u,d}}^N$ do depend on z . However, for $1 < z < 2$, their central values vary within the $1-\sigma$ ranges quoted in Table 3. Specifically, for $z = 1(2)$, we find $f_{T_u}^p = 0.015 \pm 0.004$ (0.020 ± 0.005) and $f_{T_d}^p = 0.034 \pm 0.008$ (0.023 ± 0.006).

⁸ As we noted above, the uncertainty due to B_d^p/B_u^p and z may be more important in models where the spin-independent scattering occurs primarily off u and d quarks.

We have also considered the impact of recent calculations of the heavy-quark scalar density matrix elements $\langle N|\bar{c}c, \bar{b}b, \bar{t}t|N\rangle$. The spread in lattice and phenomenological estimates of $\sigma_c = m_c \langle N|\bar{c}c|N\rangle$ is quite large, and potentially a large source of uncertainty in σ_{SI} . That said, the possible range of σ_c includes the value found to $\mathcal{O}(\alpha_s^3)$ in QCD perturbation theory. The values of the $f_{T_{c,b,t}}^N$ that we find using the $\mathcal{O}(\alpha_s^3)$ perturbative calculations of σ_c, σ_b and σ_t are shown in the last three columns of Table 3. Using the full six-quark expression for σ_{SI}^p , we find an enhancement of the cross section compared to the leading-order three-flavour approximation that is about 10% for the CMSSM fixed-point benchmark point that we have studied. We note, however, that the uncertainties in the leading-order three-quark approximation and the $\mathcal{O}(\alpha_s^3)$ six-flavour calculation overlap: $\sigma_{SI}^p = (1.25 \pm 0.13) \times 10^{-9}$ pb (three quarks) vs $\sigma_{SI}^p = (1.38 \pm 0.17) \times 10^{-9}$ pb (six quarks). As already mentioned, we consider the latter, using the estimates (24, 25, 33) and (35), to be the best approximation to the spin-independent WIMP scattering cross section currently available. As also mentioned above, we consider the spin-dependent WIMP scattering cross section to be relatively well understood.

For the future, we look forward to further refinements of calculations of $\Sigma_{\pi N}$ and σ_s using first-principles lattice techniques as well as phenomenological inputs, recalling that these are the dominant sources of uncertainty in σ_{SI} , if one accepts the perturbative calculation of σ_c . We also look forward to more accurate lattice calculations of σ_c , so as to check the accuracy of this perturbative calculation. Lattice calculations have made great progress over the past decade, but improvement is still desirable.

Acknowledgements We would like to thank M. Hoferichter, F. Kahlhoefer, U. Meißner and M. Voloshin for useful discussions. The work of JE was supported partly by the United Kingdom STFC Grant ST/P000258/1 and partly by the Estonian Research Council via a Mobil-itas Plus grant. The work of N.N. was supported by the Grant-in-Aid for Scientific Research (No.17K14270). The work of K.A.O. was supported in part by DOE grant DE-SC0011842 at the University of Minnesota.

Open Access This article is distributed under the terms of the Creative Commons Attribution 4.0 International License (<http://creativecommons.org/licenses/by/4.0/>), which permits unrestricted use, distribution, and reproduction in any medium, provided you give appropriate credit to the original author(s) and the source, provide a link to the Creative Commons license, and indicate if changes were made.

Funded by SCOAP³.

References

1. M.W. Goodman, E. Witten, Phys. Rev. D **31**, 3059 (1985)
2. D.S. Akerib et al., LUX Collaboration. Phys. Rev. Lett. **118**(2), 021303 (2017). [arXiv:1608.07648](https://arxiv.org/abs/1608.07648) [astro-ph.CO]
3. E. Aprile et al., XENON Collaboration. Phys. Rev. Lett. **119**(18), 181301 (2017). [arXiv:1705.06655](https://arxiv.org/abs/1705.06655) [astro-ph.CO]

4. X. Cui et al., PandaX-II Collaboration. Phys. Rev. Lett. **119**(18), 181302 (2017). [arXiv:1708.06917](#) [astro-ph.CO]
5. J. Billard, L. Strigari, E. Figueroa-Feliciano, Phys. Rev. D **89**(2), 023524 (2014). [arXiv:1307.5458](#) [hep-ph]
6. P. Cushman, C. Galbiati, D.N. McKinsey, H. Robertson, T.M.P. Tait, D. Bauer, A. Borgland, B. Cabrera, et al., *Snowmass Working Group Report: WIMP Dark Matter Direct Detection*. [arXiv:1310.8327](#) [hep-ex]
7. T. Falk, A. Ferstl, K.A. Olive, Phys. Rev. D **59**, 055009 (1999) [Erratum-ibid. D **60**, 119904 (1999)]. [arXiv:hep-ph/9806413](#)
8. T. Falk, A. Ferstl, K.A. Olive, Astropart. Phys. **13**, 301 (2000). [arXiv:hep-ph/9908311](#)
9. J.R. Ellis, A. Ferstl, K.A. Olive, Phys. Lett. B **481**, 304 (2000). [arXiv:hep-ph/0001005](#)
10. V. Baru, C. Hanhart, M. Hoferichter, B. Kubis, A. Nogga, D.R. Phillips, Phys. Lett. B **694**, 473 (2011). [arXiv:1003.4444](#) [nucl-th]
11. V. Baru, C. Hanhart, M. Hoferichter, B. Kubis, A. Nogga, D.R. Phillips, Nucl. Phys. A **872**, 69 (2011). [arXiv:1107.5509](#) [nucl-th]
12. A. Bottino, F. Donato, N. Fornengo, S. Scopel, Astropart. Phys. **13**, 215 (2000). [arXiv:hep-ph/9909228](#)
13. A. Bottino, F. Donato, N. Fornengo, S. Scopel, Astropart. Phys. **18**, 205 (2002). [arXiv:hep-ph/0111229](#)
14. J.R. Ellis, K.A. Olive, Y. Santoso, V.C. Spanos, Phys. Rev. D **71**, 095007 (2005). [hep-ph/0502001]
15. J.R. Ellis, K.A. Olive, C. Savage, Phys. Rev. D **77**, 065026 (2008). [arXiv:0801.3656](#) [hep-ph]
16. J.M. Alarcón, L.S. Geng, J. Martin Camalich, J.A. Oller, Phys. Lett. B **730**, 342 (2014). [arXiv:1209.2870](#) [hep-ph]
17. J.L. Feng, K.T. Matchev, T. Moroi, Phys. Rev. Lett. **84**, 2322 (2000). [arXiv:hep-ph/9908309](#)
18. H. Baer, T. Krupovnickas, S. Profumo, P. Ullio, JHEP **0510**, 020 (2005). [arXiv:hep-ph/0507282](#)
19. J.L. Feng, K.T. Matchev, D. Sanford, Phys. Rev. D **85**, 075007 (2012). [arXiv:1112.3021](#) [hep-ph]
20. P. Draper, J. Feng, P. Kant, S. Profumo, D. Sanford, Phys. Rev. D **88**, 015025 (2013). [arXiv:1304.1159](#) [hep-ph]
21. M. Drees, M.M. Nojiri, Phys. Rev. D **47**, 376 (1993). [arXiv:hep-ph/9207234](#)
22. J.D. Wells, G.L. Kane, C.F. Kolda, L. Roszkowski, Phys. Rev. D **49**, 6173 (1994). [arXiv:hep-ph/9312272](#)
23. J.R. Ellis, K.A. Olive, Y. Santoso, V.C. Spanos, Phys. Lett. B **565**, 176 (2003). [arXiv:hep-ph/0303043](#)
24. H. Baer, C. Balazs, JCAP **0305**, 006 (2003). [arXiv:hep-ph/0303114](#)
25. A.B. Lahanas, D.V. Nanopoulos, Phys. Lett. B **568**, 55 (2003). [arXiv:hep-ph/0303130](#)
26. U. Chattopadhyay, A. Corsetti, P. Nath, Phys. Rev. D **68**, 035005 (2003). [arXiv:hep-ph/0303201](#)
27. J. Ellis, K.A. Olive, [arXiv:1001.3651](#) [astro-ph.CO], published in *Particle dark matter*, ed. G. Bertone, pp. 142–163
28. J. Ellis, F. Luo, K.A. Olive, P. Sandick, Eur. Phys. J. C **73**(4), 2403 (2013). [arXiv:1212.4476](#) [hep-ph]
29. J. Ellis, J.L. Evans, F. Luo, N. Nagata, K.A. Olive, P. Sandick, Eur. Phys. J. C **76**(1), 8 (2016). [arXiv:1509.08838](#) [hep-ph]
30. J. Ellis, J.L. Evans, A. Mustafayev, N. Nagata, K.A. Olive, Eur. Phys. J. C **76**(11), 592 (2016). [arXiv:1608.05370](#) [hep-ph]
31. K. Griest, Phys. Rev. Lett. **61**, 666 (1988)
32. K. Griest, Phys. Rev. D **38**, 2357 (1988) Erratum: [Phys. Rev. D **39**, 3802 (1989)]
33. R. Barbieri, M. Frigeni, G.F. Giudice, Nucl. Phys. B **313**, 725 (1989)
34. J.R. Ellis, R.A. Flores, Phys. Lett. B **300**, 175 (1993)
35. M. Drees, M. Nojiri, Phys. Rev. D **48**, 3483 (1993). [arXiv:hep-ph/9307208](#)
36. G. Jungman, M. Kamionkowski, K. Griest, Phys. Rep. **267**, 195 (1996)
37. J. Hisano, K. Ishiwata, N. Nagata, Phys. Rev. D **82**, 115007 (2010). [arXiv:1007.2601](#) [hep-ph]
38. J. Hisano, R. Nagai, N. Nagata, JHEP **1505**, 037 (2015). [arXiv:1502.02244](#) [hep-ph]
39. J. Hisano, K. Ishiwata, N. Nagata, JHEP **1506**, 097 (2015). [arXiv:1504.00915](#) [hep-ph]
40. M.A. Shifman, A.I. Vainshtein, V.I. Zakharov, Phys. Lett. **78B**, 443 (1978)
41. A.I. Vainshtein, V.I. Zakharov, M.A. Shifman, Usp. Fiz. Nauk **130**, 537 (1980)
42. E.A. Bagnaschi et al., Eur. Phys. J. C **75**, 500 (2015). [arXiv:1508.01173](#) [hep-ph]
43. H. Leutwyler, Phys. Lett. B **378**, 313 (1996). [arXiv:hep-ph/9602366](#)
44. C. Patrignani et al., Particle Data Group. Chin. Phys. C **40**(10), 100001 (2016)
45. H.Y. Cheng, Phys. Lett. B **219**, 347 (1989)
46. A. Crivellin, M. Hoferichter, M. Procura, Phys. Rev. D **89**, 054021 (2014). [arXiv:1312.4951](#) [hep-ph]
47. A. Crivellin, M. Hoferichter, M. Procura, L.C. Tunstall, JHEP **1507**, 129 (2015). [arXiv:1503.03478](#) [hep-ph]
48. A.W. Thomas, X.G. Wang, R.D. Young, Phys. Rev. C **91**(1), 015209 (2015) [arXiv:1406.4579](#) [nucl-th]
49. G.S. Bali et al., RQCD Collaboration. Phys. Rev. D **93**(9), 094504 (2016). [arXiv:1603.00827](#) [hep-lat]
50. G. Hinshaw et al., WMAP Collaboration. Astrophys. J. Suppl. **208**, 19 (2013). [arXiv:1212.5226](#) [astro-ph.CO]
51. P.A.R. Ade et al., Planck Collaboration. Astron. Astrophys. **594**, A13 (2016). [arXiv:1502.01589](#) [astro-ph.CO]
52. B. Borasoy, U.G. Meißner, Ann. Phys. **254**, 192 (1997). [hep-ph/9607432]
53. J. Gasser, H. Leutwyler, M.E. Sainio, Phys. Lett. B **253**, 252 (1991)
54. M. Knecht, PiN Newslett. **15**, 108 (1999). [arXiv:hep-ph/9912443](#)
55. M.E. Sainio, PiN Newslett. **16**, 138 (2002). [arXiv:hep-ph/0110413](#)
56. M.M. Pavan, I.I. Strakovsky, R.L. Workman, R.A. Arndt, PiN Newslett. **16**, 110 (2002). [hep-ph/0111066]
57. T. Bringmann et al. [The GAMBIT Dark Matter Workgroup], Eur. Phys. J. C **77**(12), 831 (2017). [arXiv:1705.07920](#) [hep-ph]
58. H. W. Lin. [arXiv:1112.2435](#) [hep-lat]
59. J. Giedt, A.W. Thomas, R.D. Young, Phys. Rev. Lett. **103**, 201802 (2009). [arXiv:0907.4177](#) [hep-ph]
60. M. Hoferichter, J. Ruiz de Elvira, B. Kubis, U.G. Meißner, Phys. Lett. B **760**, 74 (2016). [arXiv:1602.07688](#) [hep-lat]
61. H. Ohki et al., Phys. Rev. D **78**, 054502 (2008). [arXiv:0806.4744](#) [hep-lat]
62. J.M. Alarcón, J. Martin Camalich, J.A. Oller, Phys. Rev. D **85**, 051503 (2012). [arXiv:1110.3797](#) [hep-ph]
63. R. Horsley et al., QCDSF-UKQCD Collaboration. Phys. Rev. D **85**, 034506 (2012). [arXiv:1110.4971](#) [hep-lat]
64. G.S. Bali et al., QCDSF Collaboration. Phys. Rev. D **85**, 054502 (2012). [arXiv:1111.1600](#) [hep-lat]
65. W. Freeman et al., MILC Collaboration. Phys. Rev. D **88**, 054503 (2013). [arXiv:1204.3866](#) [hep-lat]
66. P.E. Shanahan, A.W. Thomas, R.D. Young, Phys. Rev. D **87**, 074503 (2013). [arXiv:1205.5365](#) [nucl-th]
67. G.S. Bali et al., Nucl. Phys. B **866**, 1 (2013). [arXiv:1206.7034](#) [hep-lat]
68. H. Ohki et al., JLQCD Collaboration. Phys. Rev. D **87**, 034509 (2013). [arXiv:1208.4185](#) [hep-lat]
69. X.-L. Ren, L.S. Geng, J. Martin Camalich, J. Meng, H. Toki, JHEP **1212**, 073 (2012). [arXiv:1209.3641](#) [nucl-th]
70. M. Engelhardt, Phys. Rev. D **86**, 114510 (2012). [arXiv:1210.0025](#) [hep-lat]
71. J. Stahov, H. Clement, G.J. Wagner, Phys. Lett. B **726**, 685 (2013). [arXiv:1211.1148](#) [nucl-th]

72. Y.H. Chen, D.L. Yao, H.Q. Zheng, Phys. Rev. D **87**, 054019 (2013). [arXiv:1212.1893](#) [hep-ph]
73. P. Jannackar, A. Walker-Loud, Phys. Rev. D **87**, 114510 (2013). [arXiv:1301.1114](#) [hep-lat]
74. C. Jung [RBC and UKQCD Collaborations], PoS LATTICE **2012**, 164 (2012). [arXiv:1301.5397](#) [hep-lat]
75. L. Alvarez-Ruso, T. Ledwig, J. Martin Camalich, M.J. Vicente-Vacas, Phys. Rev. D **88**(5), 054507 (2013). [arXiv:1304.0483](#) [hep-ph]
76. M. Gong et al., XQCD Collaboration. Phys. Rev. D **88**, 014503 (2013). [arXiv:1304.1194](#) [hep-ph]
77. X.L. Ren, L.S. Geng, J. Meng, Phys. Rev. D **91** (2015)(5), 051502. [arXiv:1404.4799](#) [hep-ph]
78. M. Hoferichter, J. Ruiz de Elvira, B. Kubis, U.G. Meißner, Phys. Rev. Lett. **115**, 092301 (2015). [arXiv:1506.04142](#) [hep-ph]
79. M. Hoferichter, J. Ruiz de Elvira, B. Kubis, U.G. Meißner, Phys. Rept. **625**, 1 (2016). [arXiv:1510.06039](#) [hep-ph]
80. S. Durr et al., Phys. Rev. Lett. **116**(17), 172001 (2016). [arXiv:1510.08013](#) [hep-lat]
81. Y.B. Yang et al. [xQCD Collaboration], Phys. Rev. D **94**(5), 054503 (2016). [arXiv:1511.09089](#) [hep-lat]
82. A. Abdel-Rehim et al. [ETM Collaboration], Phys. Rev. Lett. **116**(25), 252001 (2016). [arXiv:1601.01624](#) [hep-lat]
83. D.L. Yao, D. Siemens, V. Bernard, E. Epelbaum, A. M. Gasparyan, J. Gegelia, H. Krebs and U. G. Meißner, JHEP **1605** (2016) 038. [arXiv:1603.03638](#) [hep-ph]. We use the estimates of σ_s from Table VII of this paper, which are based in the determination of $\Sigma_{\pi N}$ given in [57]
84. S. Duan, C. S. An and B. Saghai, Phys. Rev. D **93**(11), 114006 (2016). [arXiv:1606.02000](#) [hep-ph]
85. C. Alexandrou and C. Kallidonis, Phys. Rev. D **96**(3), 034511 (2017). [arXiv:1704.02647](#) [hep-lat]
86. J. Ruiz de Elvira, M. Hoferichter, B. Kubis and U. G. Meißner, J. Phys. G **45**(2), 024001 (2018). [arXiv:1706.01465](#) [hep-ph]
87. X.Z. Ling, X.L. Ren, L.S. Geng, [arXiv:1710.07164](#) [hep-ph]
88. M.F.M. Lutz, Y. Heo, X.Y. Guo, [arXiv:1801.06417](#) [hep-lat]. These authors comment that they consider outdated the earlier results in A. Semke and M. F. M. Lutz, Phys. Lett. B **717**, 242 (2012). [arXiv:1202.3556](#) [hep-ph] and
89. M.F.M. Lutz, R. Bavontaweepanya, C. Kobdaj, K. Schwarz, Phys. Rev. D **90**(5), 054505 (2014). [arXiv:1401.7805](#) [hep-lat], which we therefore do not include in our analysis
90. I.P. Fernando, J.M. Alarcón and J. L. Goity. [arXiv:1804.03094](#) [hep-ph]
91. T.J. Hobbs, M. Alberg, G.A. Miller, Phys. Rev. D **96**(7), 074023 (2017). [arXiv:1707.06711](#) [hep-ph]
92. L. Vecchi. [arXiv:1312.5695](#) [hep-ph]
93. A. Kryjevski, Phys. Rev. D **70**, 094028 (2004). [hep-ph/0312196]
94. R.J. Hill, M.P. Solon, Phys. Rev. D **91**, 043505 (2015). [arXiv:1409.8290](#) [hep-ph]
95. S.J. Brodsky, A. Kusina, F. Lyonnet, I. Schienbein, H. Spiesberger, R. Vogt, Adv. High Energy Phys. **2015**, 231547 (2015). [arXiv:1504.06287](#) [hep-ph]
96. J.R. Ellis, R.A. Flores, S. Ritz, Phys. Lett. B **198**, 393 (1987)